GEOPHYSICS, VOL. 78, NO. 6 (NOVEMBER-DECEMBER 2013); P. EN117–EN127, 13 FIGS., 1 TABLE.
10.1190/GEO2012-0392.1

High-frequency seismic response during permeability reduction due to biopolymer clogging in unconsolidated porous media

Tae-Hyuk Kwon[1] and Jonathan B. Ajo-Franklin[2]

ABSTRACT

The accumulation of biopolymers in porous media, produced by stimulating either indigenous bacteria or artificially introduced microbes, readily blocks pore throats and can effectively reduce bulk permeability. Such a microbial clogging treatment can be used for selective plugging of permeable zones in reservoirs and is considered a potentially promising approach to enhance sweep efficiency for microbial enhanced oil recovery (MEOR). Monitoring in situ microbial growth, biopolymer formation, and permeability reduction in the reservoir is critical for successful application of this MEOR approach. We examined the feasibility of using seismic signatures (P-wave velocity and attenuation) for monitoring the in situ accumulation of insoluble biopolymers in unconsolidated sediments. Column experiments, which involved stimulating the sucrose metabolism of *Leuconostoc mesenteroides* and production of the biopolymer dextran, were performed while monitoring changes in permeability and seismic response using the ultrasonic pulse transmission method. We observed that *L. mesenteroides* produced a viscous biopolymer in sucrose-rich media. Accumulated dextran, occupying 4%–6% pore volume after ~20 days of growth, reduced permeability more than one order of magnitude. A negligible change in P-wave velocity was observed, indicating no or minimal change in compressive stiffness of the unconsolidated sediment during biopolymer formation. The amplitude of the P-wave signals decreased ~80% after ~20 days of biopolymer production; spectral ratio analysis in the 0.4–0.8-MHz band showed an approximate 30%–50% increase in P-wave attenuation ($1/Q_P$) due to biopolymer production. A flow-induced loss mechanism related to the combined grain/biopolymer structure appeared to be the most plausible mechanism for causing the observed increase in P-wave attenuation in the ultrasonic frequency range. Because permeability reduction is also closely linked to biopolymer volume, P-wave attenuation in the ultrasonic frequency range appears to be an effective indicator for monitoring in situ biopolymer accumulation and permeability reduction and could provide a useful proxy for regions with altered transport properties.

INTRODUCTION

Microorganisms produce a variety of compounds that are capable of mobilizing oil trapped in reservoirs and improving oil recovery (Youssef et al., 2009). Biosurfactants, solvents, miscible gases, or acids produced by microorganisms can increase oil mobility in porous media by lowering interfacial tension and/or decreasing oil viscosity. In the case of heterogeneous reservoirs undergoing water floods, one possible production enhancement approach is the selective plugging of permeable "thief zones" to enhance sweep efficiency. Bacteria commonly develop colonies on mineral surfaces of porous media by producing copious amounts of extracellular polymeric substances (EPS), which consist of protein, polysaccharides, nucleic acids, and lipids. A biofilm is a mixture of bacterial cells and EPS; the EPS in biofilms produced by certain bacteria are referred to as biopolymers. The accumulation of insoluble EPS (or biopolymers) in porous media, produced by certain bacteria under favorable growth conditions, readily blocks pore throats and can effectively reduce bulk permeability by several orders of magnitude (Taylor and Jaffé, 1990; Lappan and Fogler, 1996). Biopolymer clogging can be achieved by stimulating either indigenous bacterial populations or artificially introduced microbes with an injected

Manuscript received by the Editor 22 September 2012; revised manuscript received 18 June 2013; published online 21 October 2013.
[1]Korea Advanced Institute of Science and Technology (KAIST), Department of Civil and Environmental Engineering, Daejeon, Korea. E-mail: t.kwon@kaist.ac.kr.
[2]Lawrence Berkeley National Laboratory, Earth Sciences Division, Berkeley, California, USA. E-mail: jbajo-franklin@lbl.gov.

carbon source (e.g., sucrose). This class of microbial clogging treatment has been demonstrated in prior laboratory experiments and is considered a potentially promising avenue within the microbial enhanced oil recovery (MEOR) community (Gray et al., 2008).

However, detecting the regions of active microbial growth and monitoring biopolymer formation will be critical for successful application of this technique. Effective refinement of an injection strategy will require information on biopolymer distribution in the near-well region and deeper in the reservoir where the bulk of bypassed oil resides. Thus, developing techniques for monitoring in situ bacterial growth, biopolymer formation, and permeability reduction is essential for successful application of this MEOR approach. Considerable interest also exists in the field of biogeophysics, which focuses on the links between subsurface microbial processes and geophysical signatures as well as the potential of geophysical techniques to elucidate such microbial processes in the laboratory and in the field (Atekwana and Slater, 2009). As an example, mineral precipitation induced by microbial activities as a means of bioremediation or soil improvement has been shown to increase the shear stiffness and strength of soils and is thus easily detectable by measurement of S-wave velocity (e.g., DeJong et al., 2006; van Paassen et al., 2010). Techniques based on acoustic-wave propagation (e.g., seismic methods and sonic logging) appear to be a promising means of monitoring these pore-scale microbial processes in porous media; previous studies have demonstrated that ultrasonic P-wave measurements are sensitive to the products of microbial activities in porous media, such as biogenic gas generation (e.g., Rebata-Landa and Santamarina, 2012), biomineralization (e.g., Williams et al., 2005; DeJong et al., 2006), and biofilm formation (e.g., Davis et al., 2009, 2010). To date, the relationships between seismic response and biopolymer formation and the resulting permeability reduction have not been investigated.

Biopolymer clogging can cause significant changes in the physical properties of porous media and influence transport behavior as well as geophysical response. Prior studies have demonstrated that sandstone samples can be quickly clogged by biopolymer production through stimulation of active cultures of *Leuconostoc mesenteroides* (Lappan and Fogler, 1996; Stewart and Fogler, 2001), reducing local permeability by more than one order of magnitude in less than 24 h. *L. mesenteroides* has also been used in prior MEOR field trials, although with mixed results, possibly due to transport/flushing of the active microbial system (e.g., Jack, 1991). Few measurements exist delineating the impact of biopolymer or similar soft biological compound production on seismic response; the one pertinent sequence of studies to date (Davis et al., 2009, 2010) examines the impact of microbial growth and biofilm formation by *Pseudomonas aeruginosa* on seismic responses, and it suggests that the EPS in the biofilms generated by *P. aeruginosa* can alter seismic signatures in the ultrasonic frequency range via a significant increase in P-wave attenuation (inferred through an amplitude reduction) and a small increase in P-wave velocity. However, Davis and colleagues do not come to a definitive conclusion with regard to the physical mechanism generating the observed attenuation changes nor do they provide a quantitative relationship between EPS volume and modification in transport properties or seismic responses (Davis et al., 2009, 2010). They suggest the "sticky" effects of EPS at grain-to-grain contacts, squirt flow, and scattering as possible causes of the observed increase of seismic attenuation but were unable to eliminate any of these possibilities. Thus, to identify the link between biofilm formation and seismic responses and apply traditional effective medium models relating volume fractions of EPS to such seismic response, further extending the previous work of Davis et al. (2009, 2010), one key challenge seems to be in designing well-controlled laboratory experiments in which simultaneous monitoring of biological product quantity, transport properties, and geophysical signatures is possible.

This study examines the feasibility of using P-wave signatures (velocity and attenuation) for monitoring the in situ accumulation of insoluble bacterial biopolymers in unconsolidated sediments. Because permeability reduction is also closely linked to biopolymer volume, such a seismic signature would provide a proxy for regions with altered transport properties. Column experiments, which involved stimulation of bacterial growth of *L. mesenteroides*, production of EPS in biofilms (or biopolymer) by *L. mesenteroides*, and clogging of a porous medium, were performed while monitoring changes in permeability and P-wave response using the ultrasonic pulse transmission method. In addition, hypotheses to explain the observed changes in P-wave responses were explored by complementary experiments including direct measurement of biopolymer properties in the absence of the porous matrix.

MATERIALS AND METHODS

Model bacteria

The bacterium used in this study was *Leuconostoc mesenteroides* NRRL B-523 (American Type Culture Collection, ATCC 14935). The selection of *L. mesenteroides* was based on a variety of attractive attributes, which makes it well suited for laboratory bioclogging experiments. *L. mesenteroides* is a facultative anaerobe and grows well in nitrogen or argon atmospheres but can be cultured aerobically if required. The bacterium also has a low pathogenicity profile (biosafety level 1), which decreases hazards during laboratory and field experimentation. The cells are generally nonmotile with a coccoid morphology and an average diameter of ~600 nm (Figure 1a), which facilitates microbial transport by way of advection in porous materials. The bacteria can produce copious amounts of the insoluble biopolymer dextran (Figure 1b and 1c); the bacterial metabolism, which uses the enzyme dextransucrase to transform sucrose into insoluble dextran (biopolymer), fructose, and a variety of secondary compounds, is well characterized (Lappan and Fogler, 1994). The properties of dextran (e.g., solubility, viscosity) are dependent upon the polymer chain length, which is generally not well controlled in microbial clogging experiments. Dextran's moderate aqueous solubility leads to rapid accumulation of the insoluble product during microbial production; in this study, the insoluble dextran formed a gel phase over short time periods, becoming visible within 24 h (Figure 1d; see also Padmanabhan et al., 2003). Batch experiments in our laboratory have also confirmed that *L. mesenteroides* tolerates reservoir pressures (~30 MPa) and effectively generates dextran in these conditions. The rheological properties of the gel form of the pertinent biopolymer (dextran) have been effectively characterized in previous studies (e.g., Padmanabhan et al., 2003).

Throughout the present study, a defined growth medium containing trace minerals, vitamins, phosphate buffers, and 15 g/L sucrose (Table 1) was used to stimulate the growth of the model bacteria *L. mesenteroides* and their biopolymer under a consistent environment. The pH of the growth medium was conditioned to be 6.8

using phosphate buffers. The model bacteria were aerobically cultured in a batch reactor at 30°C, and the initial culture was stored as multiple frozen stocks at –80°C for subsequent column experiments present in this study. For the column experiments, an inoculum was aerobically grown from a frozen stock in a batch reactor with the defined growth medium at 30°C for ~48 h. The insoluble dextran produced by *L. mesenteroides* in our defined growth medium appears initially as small filaments between 10 and 100 μm in length (Figure 1); these filaments can then accumulate as porous deposits or layers in pore spaces. Aerobic and anaerobic batch experiments were performed several times under controlled growth conditions, and the morphology of the produced dextran and cultured cells were imaged by using scanning electron microscopy (SEM) and optical microscopy to confirm consistent production of biopolymers from model bacteria, as shown in Figure 1.

Column setup

An experimental column setup was designed to explore the evolution of permeability and P-wave response (velocity and attenuation) during biopolymer formation in unconsolidated sediment samples (see Figures 2–4). The transparent, rigid-walled column (acrylic; volume, 475 cm^3; internal diameter, 65.3 mm; height, 150 mm) used in this study was instrumented with one differential pressure transducer (PX409, OMEGA) and two pairs of immersion-type ultrasonic transducers (A303S-SU, Panametrics; 1 MHz). The differential pressure transducer was powered at 10 V by a DC power supply, and a data logger (34970A, Agilent) was used to record the output differential pressure values. The ultrasonic transducers were connected to an ultrasonic pulse generator, and a computer-controlled digital oscilloscope was used to acquire the received signals at the receiver ultrasonic transducers (see Figures 2 and 3). A transparent polycarbonate transfer vessel (Figure 4) was connected to a syringe pump (260D, ISCO-Teledyne) and used to inject growth media into the column as the syringe pump provided water at a constant flow rate. The pressure of the pore fluid in the column was controlled by a back-pressure regulator to keep the sediment sample water saturated and avoid bubble formation.

Procedures and measurements

A fine quartz sand (Ottawa F110; uniform grain size; mean particle diameter = 120 μm) was used as the host sediment. The fine sand column was wet packed with the fresh growth medium (Table 1) so as to remove trapped air. The sand was washed with deionized water, oven dried, and sterilized by autoclaving prior to being packed in the column. Two tests were conducted, and the porosities of the prepared sand packs were 0.38 and 0.35 for the first and second runs, respectively. An inoculum ($\sim 4 \times 10^{10}$ cells/L) was prepared from the cells aerobically grown in a batch reactor with the growth medium. 20 mL of the inoculum was injected into the column using the injection port located at the center of the sand pack to avoid local clogging in the vicinity of the nutrient injection port located at the bottom of the column and to stimulate homogeneous biopolymer formation, particularly in the P-wave monitoring zone.

Then, 100 mL of a fresh, sterile growth medium was injected at a flow rate of 2 mL/min while measuring the pressure difference between two ports located at the column every 10 s by the data logger. The baseline permeability was determined based on this pressure difference (i.e., approximately 5.25×10^{12} m^2 or ~5.3 D and 4.91×10^{-12} m^2 or ~5.0 D for the first and second runs, respectively). During this first injection, the fluid pressure inside the column was increased to 293 kPa and controlled by a back-pressure regulator installed at the outlet port. The fluid pressure was kept constant at 293 kPa throughout the experiment to dissolve microbially generated gas in aqueous solution and avoid any bubble formation in the column. Baseline acoustic measurements were also collected.

The experiment was conducted in a pulsed-flow mode; i.e., we alternated between shut-in periods and short-duration injections rather than carrying out a continuous injection. In each cycle of the process, a shut-in period of more than 48 h was allowed for the bacteria to grow and produce biopolymer without advective forces, under ambient room temperature (~20°C). After the shut-in period, the pore fluid containing old and consumed nutrients was replaced with a fresh growth medium using a syringe pump at a flow rate of 2 mL/min (i.e., a refilling period). The volume of the fresh growth media used for the refilling process was 300 mL in the first run and 200 mL in the second run (1.3–2 times of the pore volume). During this refilling process, differential pressure was monitored every 10 s by using a data logger, and the recorded values were used to calculate the evolution of permeability. In addition, the effluents were sampled and analyzed to quantify

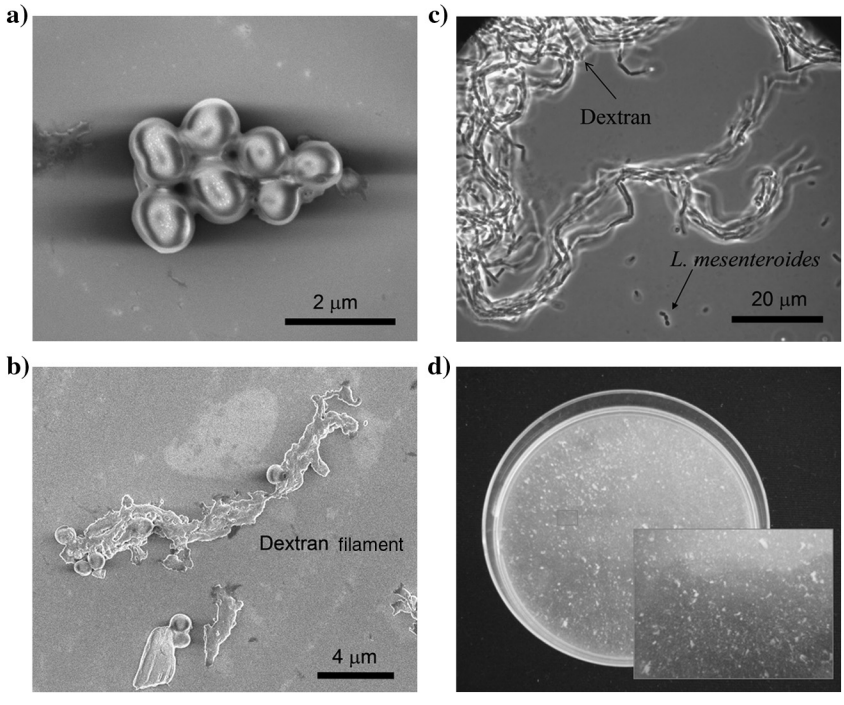

Figure 1. *L. mesenteroides* and dextran produced. (a) SEM images of cells and (b) dextran filaments with cells. An (c) optical bright-field image and (d) characterization photo of dextran in suspension produced from aerobic culture of *L. mesenteroides* in a batch reactor without a porous medium.

total inorganic carbon and total organic carbon contents (TIC/TOC analysis). Then, the organic carbon content values were used to calculate net carbon influx to the column from mass balance and to quantify the amount of dextran and biomass produced by microbial activity. This cycle of shut-in/refilling periods was repeated for the duration of the experiments, which lasted 17 and 23 days for the first and second runs, respectively.

Table 1. Composition of the defined growth medium for *L. mesenteroides*.

Compound	Concentration	Molarity
Carbon sources		
Sucrose	15 g/L	43.82 mM
Na-acetate	1 g/L	12.2 mM
$(NH_4)_3$-citrate	0.6 g/L	2.47 mM
Yeast extract	0.5 g/L	—
Trace minerals and buffer		
$MnSO_4 \cdot H_2O$	1 g/L	0.0592 mM
$MgCl_2 \cdot 6H_2O$	20 g/L	0.984 mM
Monobasic — KH_2PO_4	13.609 g/L	100 mM
Dibasic — K_2HPO_4	17.418 g/L	100 mM
Vitamins		
D-Biotin	0.02 mg/L	0.082 μM
Folic acid	0.02 mg/L	0.045 μM
Pyridoxine hydrochloride	0.01 mg/L	0.49 μM
Thiamine hydrochloride	0.05 mg/L	0.15 μM
Riboflavin	0.05 mg/L	0.13 μM
Nicotinic acid	0.05 mg/L	0.41 μM
Pantothenic acid	0.05 mg/L	0.21 μM
p-Aminobenzoic acid	0.05 mg/L	0.31 μM
Thioctic acid	0.05 mg/L	0.24 μM
Choline chloride	2.0 mg/L	14 μM
Vitamin B_{12}	0.01 mg/L	0.0074 μM

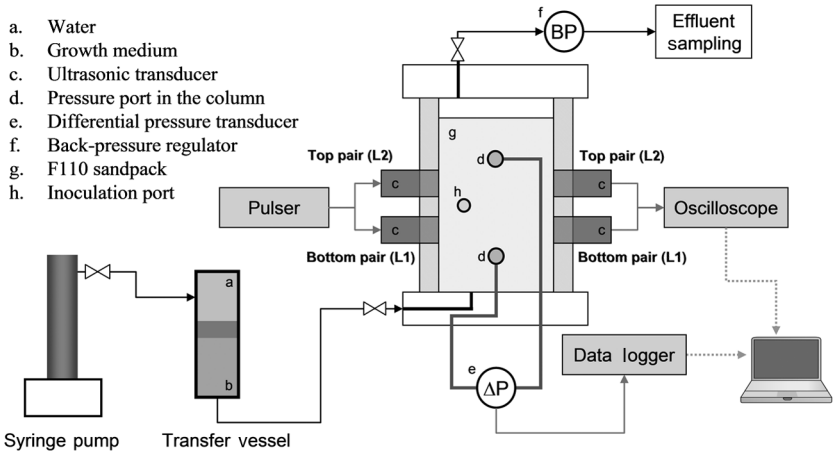

Figure 2. Column experiment setup (not to scale).

For seismic monitoring, an ultrasonic pulse generator (5077PR, Panametrics) was used to apply a high-voltage excitation signal (~400 V) to the source ultrasonic transducers. Received signals were recorded using a computer-controlled digital oscilloscope (TDS210, Tektronix) for duration of 100 μs with a sampling rate of 4 ns. Each record consisted of 64 vertical stacks (pulse repetitions) to reduce uncorrelated electrical noise. The ultrasonic signatures of the top transducer pair (L2; see Figure 2) and bottom transducer pair (L1) were automatically acquired every hour over the course of the experiments. The frequency content of the received P-wave signals ranged from 200 kHz to 1.6 MHz above the noise floor with initial centroid frequencies of ~900 kHz.

RESULTS AND ANALYSIS

Permeability reduction

The differential pressure responses obtained over the course of the refilling periods were used to estimate the reduction in permeability due to the accumulation of biopolymer in the pores of the sand pack. Permeabilities were determined from Darcy's law, while assuming single-phase flow. The insoluble dextran was treated as part of the solid phase. The fluid viscosity was assumed to be dominated by dissolved sucrose; the viscosity of the growth medium containing 15 g/L of sucrose was assumed to be 1.041×10^3 Pa · s at 20°C (Bohuon et al., 1997).

The baseline permeability was measured as 5.25×10^{-12} m^2 (or 5.3 D) for the first run. After 17 days of the first experiment, the permeability decreased to 2.25×10^{-12} m^2 (or 230 mD) due to insoluble dextran and biomass formation (Figure 5a). Likewise, the permeability decreased from 4.91×10^{-12} m^2 (or 5.0 D) to 1.09×10^{-12} m^2 (or 1.1 D) after 23 days for the second run. The insoluble EPS, herein dextran, produced by *L. mesenteroides* was the main cause of the permeability reduction (bioclogging) observed in this study. Although dextran is generally known to be somewhat soluble in water, it is reported that low-molecular-weight dextran ($M < 6000$ g mol^{-1}) is relatively insoluble compared to high-molecular-weight dextran ($M > 40000$ g mol^{-1}; Stenekes et al., 2001). Most of the dextran produced by the bacterial strain chosen in this study was observed to be present as a solid phase (see Figure 1b–1d). In addition, thin layers of sluggish biopolymer aggregates on the top of the sand pack were observed a few days after the commencement at both runs, indicating copious dextran production (Figure 6). Although the viscosity of the pore fluid in the sand pack could be higher than that of the injected fluid owing to the dissolved dextran in water, the differential pressure values measured during the refilling periods were remarkably consistent, which indicates that the refilling with the fresh growth medium did not cause a noticeable change in the viscosity of the pore fluid.

Purity of the growing culture was confirmed by observing cell morphologies via optical microscopy. In addition, the 16 S ribosomal RNA (16S rRNA) genetic sequence of the cultured bacteria in the effluent stream was analyzed to provide secondary confirmation of purity. The 16S rRNA sequence is one particular component

of the ribosome of bacterial genes that is highly conserved among different species of bacteria and is considered as a standard bacterial identification and classification technique.

Organic carbon analysis and estimation of biopolymer produced

The mass of organic carbon accumulating in the column was calculated based on the mass balance between total carbon influx and outflux. Herein, the carbon influx was determined from the injection volume of fresh growth media during refilling processes. The carbon outflux was calculated from the volume of the effluents and their organic carbon concentrations of the effluents, which were determined by TIC/TOC analyses. Inorganic carbon content in the effluent stream was determined to be insignificant, i.e., less than 5 ppm. Thereafter, the mass of organic carbon accumulating in the column was converted into the mass of dextran using the mass ratio of carbon to dextran ($\chi = 0.444$; note that the generic formula for dextran is $(C_6H_{10}O_5)_n \cdot OH_2$). As denoted by n in the generic formula, dextran shows a broad distribution of molecular sizes, varying the density of dextran depending on the length of glucosidic linkage between glucose molecules (Naessens et al., 2005). The average molecular weight of dextran is affected by the growth conditions of *L. mesenteroides* (e.g., pH, temperature, and aqueous chemistry; Naessens et al., 2005). In this study, the average density of dextran was measured as 1.5 g/cm^3, based on a pycnometer test performed on purified dextran (i.e., 9000–11,000 average molecular weight, Sigma-Aldrich). Thus, the volumetric fraction of dextran in pore spaces (hereafter, dextran pore saturation S_{dex}) was calculated using the measured dextran density value of 1.5 g/cm^3, as follows:

$$S_{dex} = \frac{V_{dex}}{V_p} = \frac{\rho_{dex} M_{dex}}{\phi V_{sed}} = \frac{\rho_{dex}}{\phi V_{sed}} \cdot \frac{(\text{outflux} - \text{influx})_{carbon}}{\chi}, \quad (1)$$

where V, M, and ρ represent the volume, mass, and density of each phase, respectively, and ϕ is the initial porosity of the sand pack. Subscripts are used to denote constituents of porous media: dex for dextran, p for pore spaces, sed for a sand-pack sample. Figure 5b shows the estimated pore saturation of dextran over the course of the experiments. The final dextran pore saturations are estimated to be approximately 5.1% and 3.9% in the first and second tests, respectively. The bacterial growth conditions in the two tests, particularly pH and sucrose availability, were kept constant; the chemically defined growth medium contained 15 g/L sucrose and was buffered at pH 6.8 (Table 1). Active temperature control was not used in the experiment, but ambient diurnal variations in the room were limited to ~2°C. Note that the calculation assumes that the net influx of carbon is 100% converted to dextran and the amount of carbon used to produce biomass, e.g., cells, is insignificant compared to the carbon used for dextran. Also, it should be noted that this calculation neglects the biomass component of TOC; direct cell counts and optical density measurements at a wavelength of 600 nm (i.e., OD600 measurements) to determine cell density were problematic due to the optical effects of insoluble dextran, as shown in Figure 1c. The combination of such assumptions and the inability to separate dextran from biomass means that some uncertainty exists in our estimates of dextran pore saturation. For instance, if the dextran density is assumed to be the same with the density of water, 1.0 g/cm^3, which we presume as a lower bound, the dextran pore saturations are estimated to be ~7.7% and ~5.8% for the first and second tests, respectively. Thus, the variations of the dextran pore saturation were less than 3% in our data range.

Seismic responses — Velocity and attenuation analyses

Figure 7a and 7b shows the continuous evolution of the primary P-wave arrivals recorded by the bottom source/receiver pair (L1) for the entire first and second experimental runs (E1 and E2), respectively. Both runs resulted in similar seismic data sets. Several data

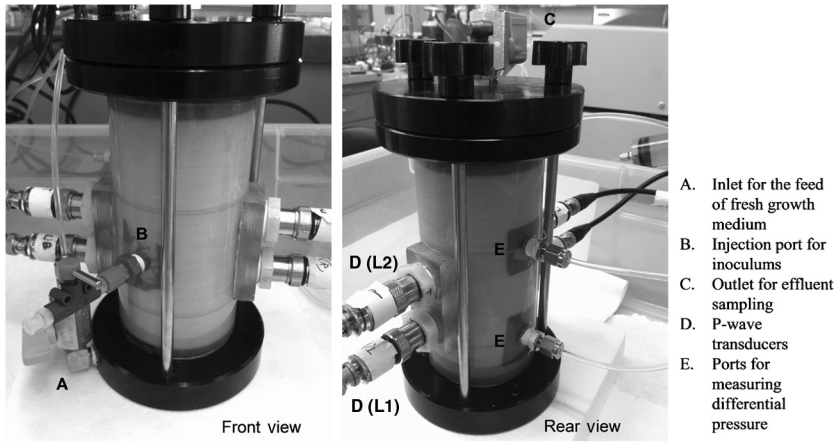

Figure 3. Photographs of the column used.

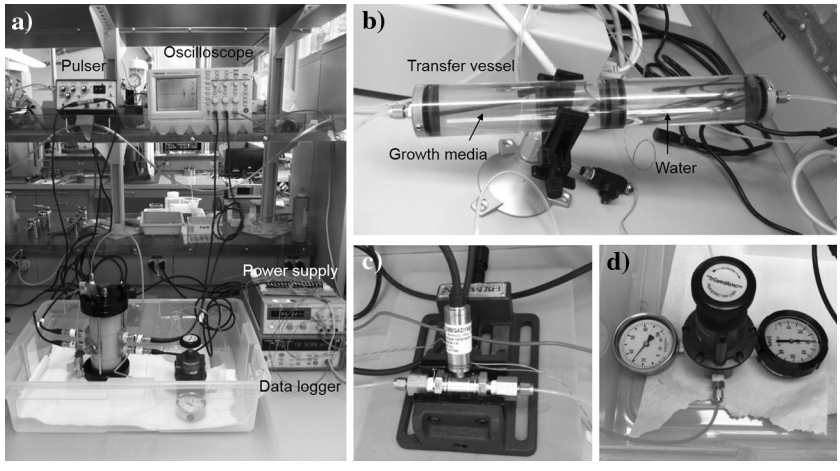

Figure 4. (a) Photographs of the test setup, (b) a transfer vessel, (c) a differential transducer, and (d) a back-pressure regulator used.

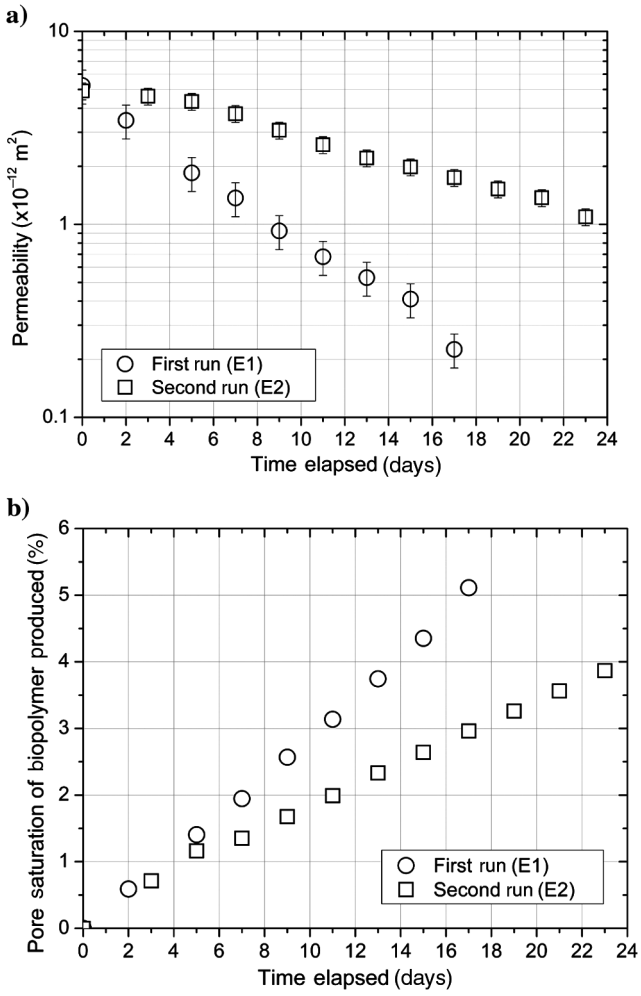

Figure 5. Changes in (a) permeability and (b) pore saturation of dextran with time.

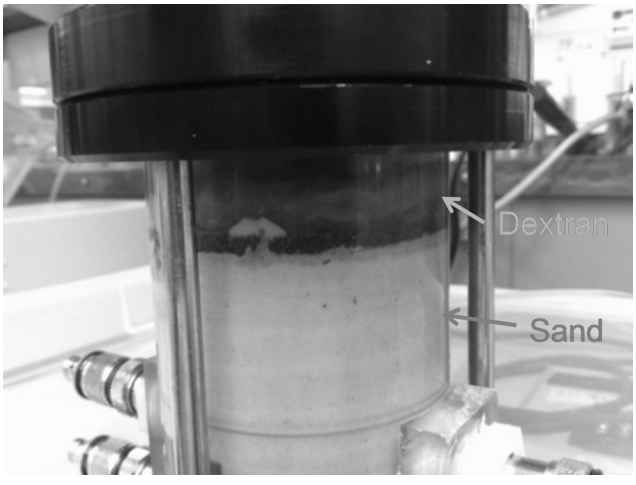

Figure 6. Dextran produced by *L. mesenteroides* and deposited on the top of the sand.

gaps exist due to temporary software problems. Only small changes in apparent velocity occurred, but a consistent decrease in signal amplitude was evident. Small variations in arrival time are evident and seem to be linked to the media replacement cycle.

Velocity analysis

All waveforms (438 data sets for each S/R pair from the first run and 684 data sets from the second run) were hand picked, and the picks were refined using waveform crosscorrelation. Calibration data sets (head-to-head and water reference) were acquired to correct for system time delays and transducer offset uncertainty. Figure 7c depicts the changes in V_P over the courses of the first run (E1, red) and the second run (E2, blue) for the bottom (L1, a diamond) and top (L2, a cross) S/R pairs. P-wave velocity is remarkably constant, varying by a maximum of ~20 m/s or about 1%, while P-wave velocity measured in the second run was higher than the values in the first run because of the lower porosity of the sand pack used for the second run. This observation demonstrates that the gel-like biopolymer does not stiffen the porous frame, even at low effective stress conditions. Although the frequency content was in the range of 0.1–2 MHz, most of the recorded energy was in a narrow band slightly below the transducer resonance frequency (1 MHz), and the content useful for analysis spanned less than a decade of frequency (0.4–1 MHz, see Figure 8). To evaluate

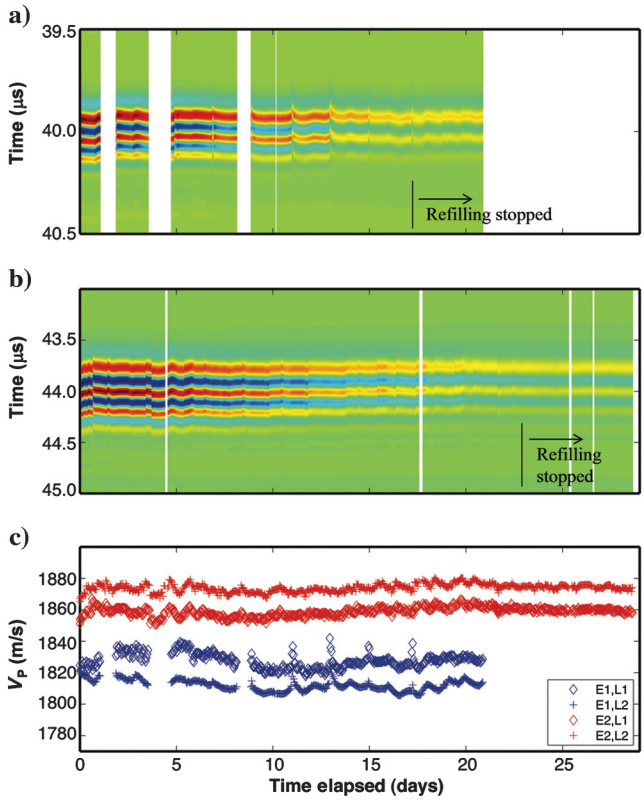

Figure 7. (a) P-wave signatures of the bottom pair (L1) over the course of the first column experiment (E1), (b) P-wave signatures of the bottom pair (L1) over the course of the second column experiment (E2), and (c) P-wave velocity with time. Note that L1 indicates the data received from the bottom pair of the ultrasonic transducers, while L2 represents the top pair.

possible velocity dispersion in the waveform data sets, band-passed versions of the data set over narrow windows (20-kHz bins) were prepared, and differential travel times were computed via crosscorrelation for each band. Over the 0.4–1 MHz range, the narrowband velocities were found to differ by less than 0.5% from the broadband velocity estimates, suggesting that velocity dispersion is not a crucial component of travel-time analysis for this particular experimental configuration.

Attenuation analysis

After velocity analysis, a careful examination of amplitude variation was conducted. All waveforms were flattened to the first arrival, and a Hamming window was applied to isolate the first two cycles of the transmitted pulse. Peak amplitudes were calculated across the windowed waveform; Figure 9a shows the changes in amplitudes of top and bottom pairs (L1 and L2) for both runs (E1 and E2). As can be seen, amplitudes for both pairs were reduced by ~80% during biopolymer production with each media reinjection producing another increase in attenuation. This observation was confirmed in the data set obtained from the second run (E2). A complementary evaluation of attenuation behavior was made using the centroid-shift method (Quan and Harris, 1997). Results shown in Figure 9b indicate progressive decreases in centroid frequency from ~900 to between 800 and 700 kHz, a clear confirmation of an active attenuative process.

The same windowed waveforms were analyzed for changes in Q using the spectral ratio method (Toksöz et al., 1979; Sears and Bonner, 1981). For the spectral ratio calculations, the column filled with deionized water (of known Q) was used to generate a mid-Q reference waveform; this was preferred to a high-Q solid reference because the exact transducer geometry and spacing was preserved. Q estimates were performed using the 400–800 kHz band. Figure 9c shows a progressive increase in attenuation ($1/Q_P$) from ~0.025 to 0.04 during dextran production, which corresponds to a decrease in Q_P values from 38 to 25 in the first run. In the second run, the P-wave attenuation ($1/Q_P$) is estimated to increase from ~0.024 to 0.03, which corresponds to a decrease in Q_P values from 41 to 32.

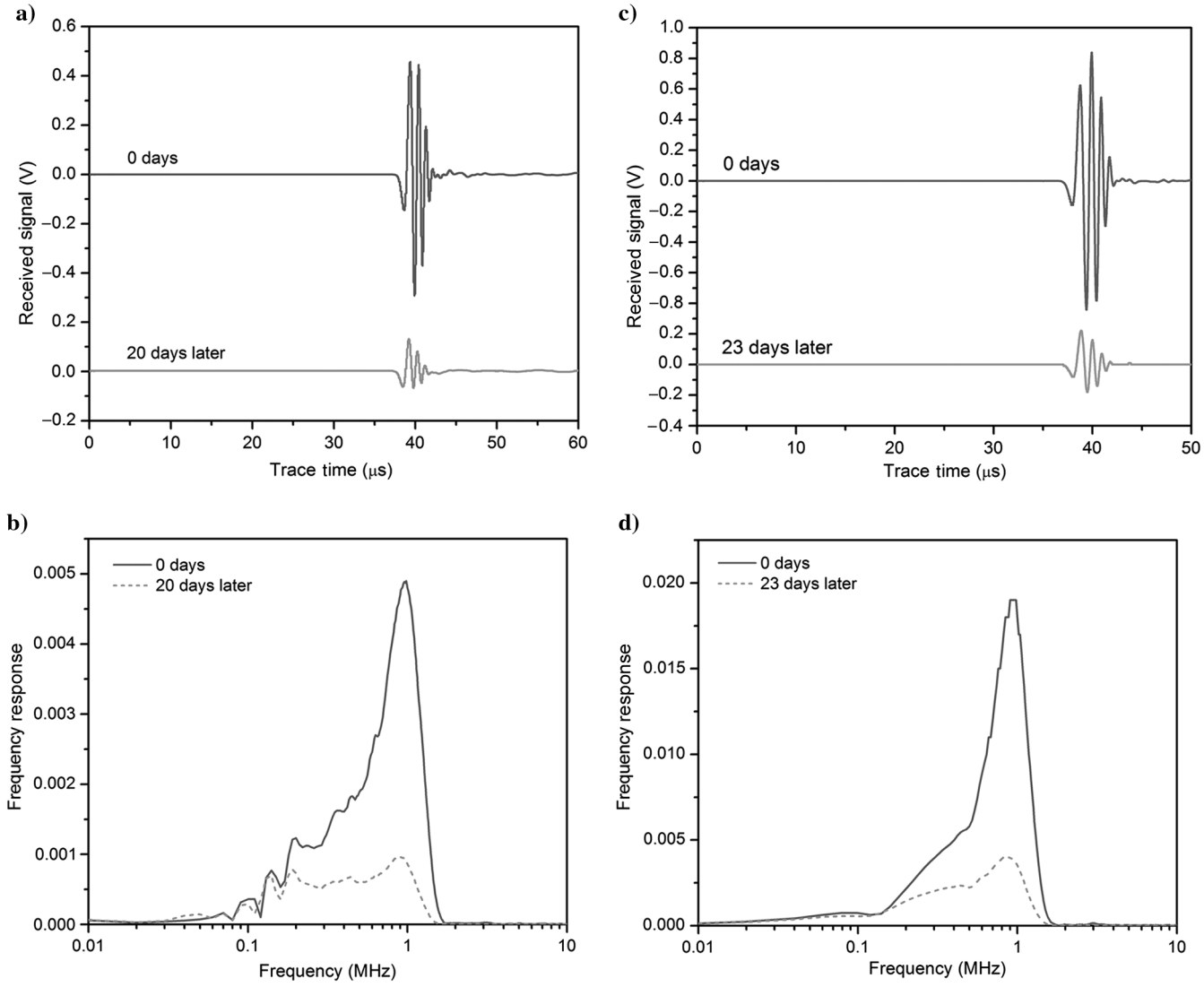

Figure 8. Recorded signals by the bottom pair (L1) and the power spectrums in the beginning and in the end of the (a, b) first and (c, d) second experiments.

The baseline Q_P values were broadly consistent with previous ultrasonic Q_P measurements performed on fine sand samples at low pressures (see Prasad and Meissner, 1992). Our results also agree with and validate the measurements of Davis et al. (2009, 2010), who observed similar attenuation changes (inferred through amplitude reduction) during stimulation of a pure culture of *P. aeruginosa*.

The refilling process (injection of fresh growth media and permeability measurements) stopped after 17 days for the first run and 23 days for the second run (Figure 5). However, seismic measurements were acquired for 21 days for the first run and 28 days for the second run to verify the possible degradation of dextran by microbes when the nutrient supply was exhausted (Figure 7). Seismic wave signatures were observed to be consistent and unchanged after stopping the refilling process (e.g., see the data from day 18 to day 21 in Figure 7a and from day 24 to day 28 in Figure 7b), indicating no dextran degradation caused by the microbes under nutrient-limited conditions.

DISCUSSION

Seismic energy loss mechanism due to biopolymer formation

Several alternative hypotheses for a possible seismic energy loss mechanism due to biopolymer formation were explored, including (1) the production of gas, (2) viscous effects within biopolymer aggregates, and (3) a flow-induced loss mechanism related to the combined grain/biopolymer structure. Although no gas generation was visible during the experiments, the potential presence of gas was examined by comparing P-wave responses when pore pressure doubled (from 207 to 414 kPa; see Figure 10). Increasing pore pressure will redissolve small gas bubbles or reduce the bubble size, generating an increase in velocity and a decrease in attenuation (Anderson and Hampton, 1980; Rebata-Landa and Santamarina, 2012). Also, any change in bubble size is expected to cause dispersion behavior to vary and will be visible in P-wave amplitude or spectral response (Anderson and Hampton, 1980). If the gas bubble size decreases, the dispersive regime and the central frequency will shift toward higher frequencies (van Dalen et al., 2010). However, no or minimal amplitude changes were observed during the pore pressure cycle, which indicates that the effect of the gas bubble presence was negligible.

Because prior experiments examining aqueous dextran solutions (rather than insoluble gels) have shown some degree of intrinsic relaxation in the ultrasonic range (e.g., Kato et al., 1980), a complementary water-dextran monitoring test was also performed without a porous medium in which dextran was produced in a liquid phase by an active *L. mesenteroides* culture. This test was conducted for 17 days while refilling with fresh media every 48 h to examine the second hypothesis that an increase in fluid viscosity due to the biopolymer could result in intrinsic relaxation in biopolymer aggregates. A substantial volume of insoluble dextran was generated in this unstirred batch experiment; nearly 40% of the ultrasonic transmission path was occupied by the biopolymer gel (Figure 11). However, the P-wave velocity and amplitude were observed to be relatively constant throughout the experiment (see Figure 12). Therefore, the viscous effect within the biopolymer aggregates (intrinsic relaxation) seems to be minimal over the frequency band we used. Additionally, because biogenic gas production should be equivalent in the absence of the granular matrix, this experiment also demonstrates the absence of a gas-related loss mechanism. The minimal velocity and amplitude contrasts between the dextran gel and water suggest that a scattering mechanism (scattering off of dextran patches) would be unlikely.

As a wave propagates through a fluid-saturated porous medium, movement of the pore fluid relative to the frame (or skeleton) causes

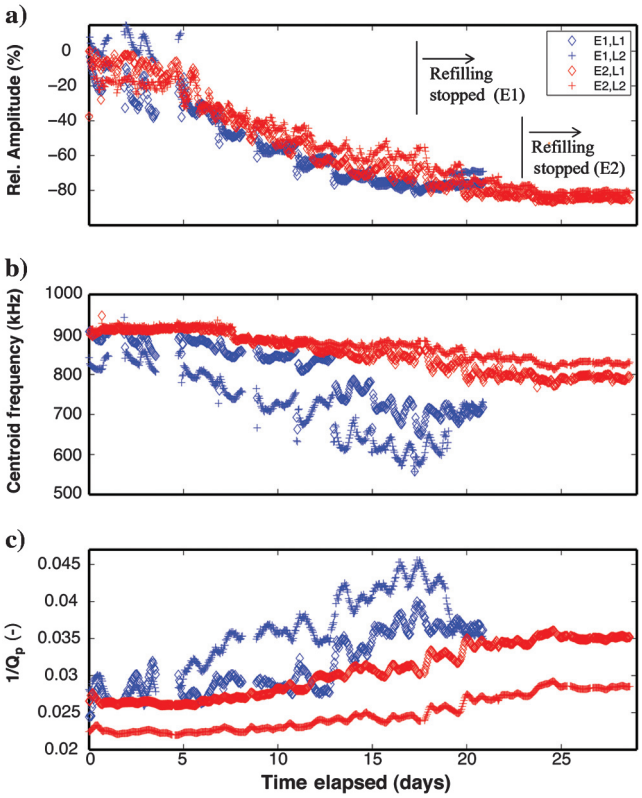

Figure 9. (a) Relative amplitude changes to the initial amplitudes, (b) centroid frequency changes, and (c) attenuation ($1/Q_P$) changes over a course of the first and second column experiments (E1 and E2). Note that L1 indicates the data received from the bottom pair of the ultrasonic transducers, while L2 represents the top pair.

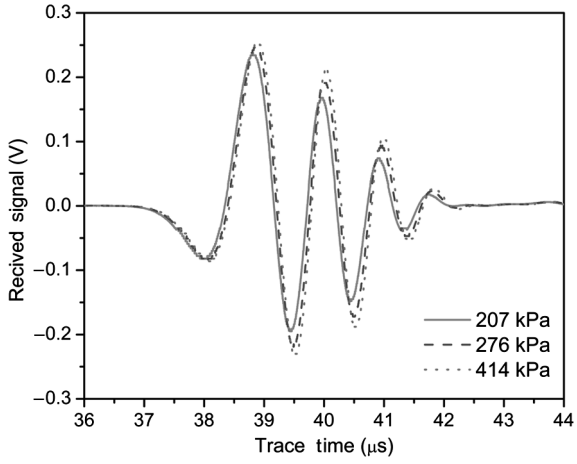

Figure 10. Received P-wave signals from the pressure cycle test.

seismic energy loss. One plausible loss mechanism is a flow-induced loss mechanism related to the combined grain/biopolymer structure. Johnson et al. (1987) show that the seismic attenuation at high frequencies was inversely proportional to the low-frequency permeability and partially controlled by pore throat roughness; a slight modification of their derivation yields the power law relation

$$\frac{1}{Q_P} \propto \left[\frac{1}{K^{1/2}}\left(\frac{2\eta}{\rho_f \omega}\right)^{1/2}\right]^{3-\delta}, \tag{2}$$

where K is the permeability, η is the viscosity, ρ_f is the fluid density, ω is the angular frequency, and δ is a fractal dimension representing the roughness of the fluid/grain contact or pore throat, a value greater than 2 but less than 3. The physical meaning of this formulation, suggested in Johnson et al. (1987), is that increased contact area between solids and water in fractally rough surfaces induces greater energy losses during wave-induced flow. In our particular case, this fractal dimension can be thought to represent the roughness of the internal dextran microstructure. Dextran produced by *L. mesenteroides* is known to have microscale pores (e.g., Shukla et al., 2011) and complicated 3D structures (see Figure 1c). Among the terms in Johnson et al. (1987)'s expression, we could not directly measure the viscosity η or the fractal dimension δ during our experiments; however, an equation of this form seems to provide some meaningful insight to the high-frequency attenuation phenomena observed in this study. However, at field seismic frequencies (1–100 Hz), the flow-induced attenuation mechanism may become less significant than that at a high frequency. Thus, heterogeneity in the medium, such as dual porosity or patchy distribution of the biopolymer, might be more relevant to attenuation mechanism during biopolymer (or biofilm) growth in porous media.

Alternative models may also exist to explain the measured changes in attenuation. The squirt flow (Mavko and Nur, 1979) and combined Biot/squirt (BISQ) models (e.g., Dvorkin et al., 1994) have often been effectively used to model attenuation effects induced at high frequencies; the squirt model posits that seismic losses are due to relative fluid motion in small cracks. Unfortunately, the complexity of the sand/gel/water system precludes straightforward adaptation of the squirt mechanism because it is unclear how crack properties would be altered by the semisolid gel phase.

Correlations between permeability, seismic attenuation, and dextran saturation

Figure 13a and 13b shows the relative changes in permeability and attenuation as a function of the pore saturation of biopolymer. The reduction in permeability is closely linked to biopolymer volume in pores (Figure 13a). Such permeability reduction is the result of the shear detachment of biopolymers from mineral surfaces and mechanical blocking of pore throats as well as the porosity reduction by accumulated biopolymers. A small amount of detached biopolymers can occlude pore throats and reduce permeability significantly; e.g., 5% pore saturation of biopolymers can reduce the permeability by one order of magnitude. Also, it appears that the extent of the increase of the high-frequency P-wave attenuation is proportional to the quantity of biopolymer when the pore saturation is less than 6% (Figure 13b). The increase in high-frequency attenuation is thought to be because of a combination of decreased permeability and increased fractal surface roughness due to biopolymer production in the porous medium. Although the permeability and attenuation results from the two tests exhibit a range of values with a given dextran pore saturation, as shown in Figure 13a and 13b, general trends, in which the production of a small amount of dextran (4%–5% of pore volume) reduced the permeability by one order of magnitude and increased the attenuation

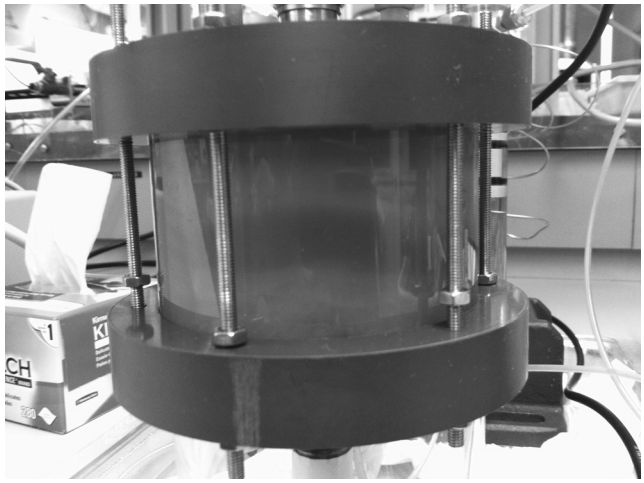

Figure 11. A photograph of the column containing a water-dextran mixture after 17 days of the experiment without a porous medium.

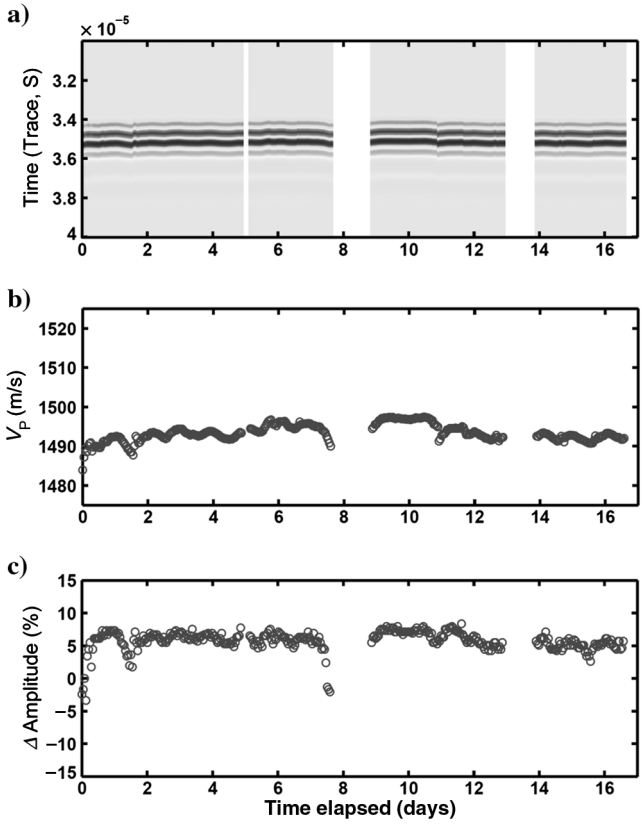

Figure 12. Seismic responses of water-dextran mixtures during dextran production without a porous medium. (a) P-wave signatures of received signals, (b) P-wave velocity, and (c) relative amplitude changes to the initial amplitudes.

($1/Q_P$) by approximately 30%–50%, can be captured. Slightly larger reductions in permeability and increases in attenuation were obtained for a given pore saturation of dextran in the first run, compared with the results from the second run. The scatter in the data is assumed to be caused by heterogeneous distribution of dextran within the column.

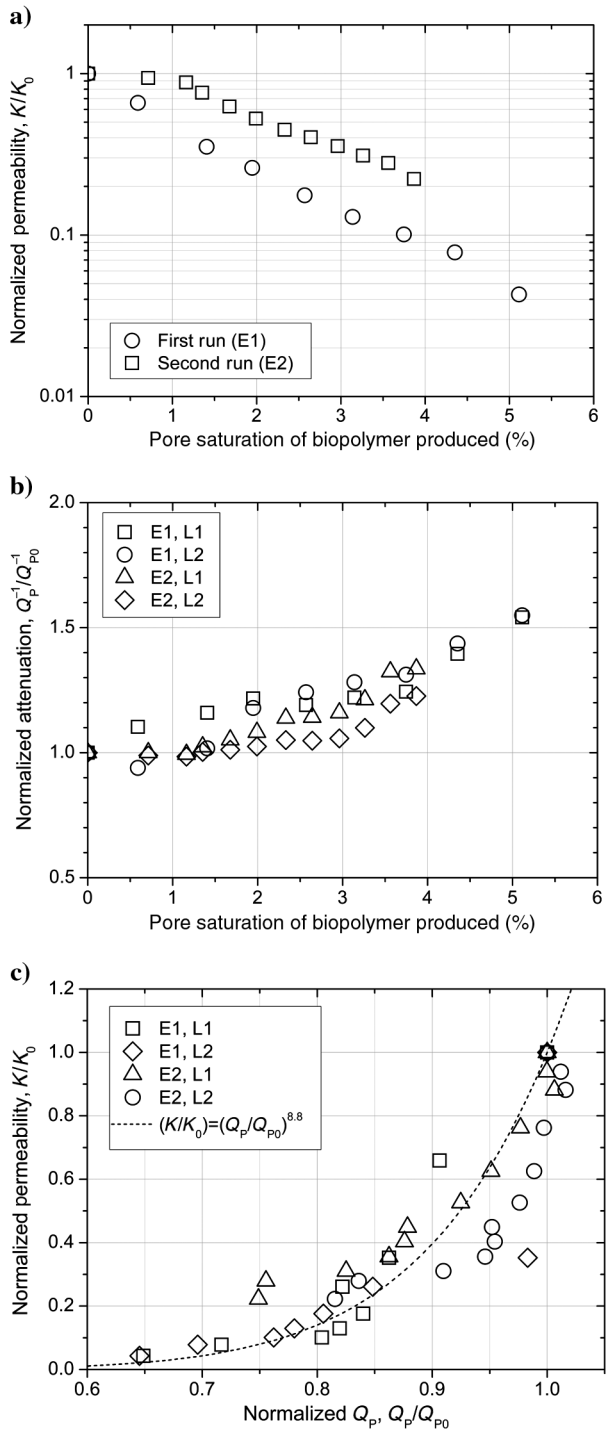

Figure 13. (a) Normalized permeability by initial permeability (K/K_0) versus pore saturation of biopolymer, (b) normalized attenuation by initial attenuation (Q_P^{-1}/Q_{P0}^{-1}) versus pore saturation of biopolymer, and (c) normalized permeability versus normalized Q_P.

Figure 13c shows a plot of normalized permeability (K/K_0) against normalized Q_P value (Q_P/Q_{P0}). We found that the permeability variations could be related to Q_P by a power law:

$$\frac{K}{K_0} = \left(\frac{Q_P}{Q_{P0}}\right)^{8.8}. \tag{3}$$

The use of such a power law formulation can be loosely justified by the fractal loss model described previously, assuming the insoluble dextran is treated as part of the grain material rather than as a viscous fluid. A more complete investigation of the permeability/fractal loss hypothesis will require direct measurement of a fractal dimension δ, a value accessible through scattering experiments using either visible light or neutrons (e.g., Radlinski et al., 1999).

CONCLUSIONS

This study examined the feasibility of using seismic signatures (P-wave velocity and attenuation) for monitoring the accumulation of insoluble biopolymers in unconsolidated sediments, using increased attenuation as a proxy for decreased permeability. Two column experiments that involved stimulating the sucrose metabolism of *L. mesenteroides* and production of the biopolymer dextran were performed while monitoring changes in permeability and seismic response using the ultrasonic pulse transmission method. The main findings are as follows: 1) Accumulated dextran, a biopolymer produced by *L. mesenteroides* in sucrose-rich media, reduced permeability more than one order of magnitude after ~20 days of growth while occupying 4%–5% pore volume. 2) A negligible change in P-wave velocity, less than 2% variation, was observed during biopolymer formation, demonstrating that the gel-like biopolymer does not noticeably stiffen the frame, not even at very low effective stress conditions. 3) The amplitude of P-wave signals decreased ~80% after ~20 days of biopolymer production, and at the same time the centroid frequency progressively decreased from ~900 to 700 or to 800-kHz, both of which confirm an active attenuative process. The spectral ratio calculations in the 400–800 kHz band showed progressive increases in P-wave attenuation ($1/Q_P$) from ~0.025 to 0.04 ($1/Q_P$) for the first run and from ~0.024 to 0.03 for the second run. 4) Via complementary experiments, the effect of the gas produced by sucrose-metabolism of *L. mesenteroides* and the viscous effect within biopolymer aggregates were found to be insignificant for causing the observed seismic energy loss during the formation of this particular type of biopolymer. 5) A flow-induced loss mechanism based on the fractally rough surfaces of the produced dextran deposits is thought to be the most plausible mechanism for causing the observed increase in P-wave attenuation in the ultrasonic frequency range. It can be hypothesized that the combination of the permeability reduction and the increased fractal surface roughness due to complicated internal micropore structures of the accumulated dextran increases seismic losses at high frequencies.

Because permeability reduction is closely linked to biopolymer volume, P-wave attenuation in the ultrasonic frequency range appears to be a good indicator for monitoring permeability reduction and would provide a useful proxy for regions with altered transport properties by this particular class of biopolymers. Before adoption

in field monitoring, lower-frequency measurements seem warranted because of the strong frequency dependence of flow-induced loss mechanisms.

ACKNOWLEDGMENTS

We would like to thank J. Carcione, L. V. Socco, E. Atekwana, T. Nemeth, and two anonymous reviewers for valuable comments and suggestions. We would also like to thank R. Chakraborty (Lawrence Berkeley National Laboratory [LBNL]) for assistance in culturing and microbial analysis, B. Bonner (LBNL) for suggestions during data analysis, and J. G. Berryman for valuable comments on the manuscript. Support for this research was provided by the Energy Biosciences Institute.

REFERENCES

Anderson, A. L., and L. D. Hampton, 1980, Acoustics of gas-bearing sediments I. Background: Journal of the Acoustical Society of America, **67**, 1865–1889, doi: 10.1121/1.384453.

Atekwana, E. A., and L. D. Slater, 2009, Biogeophysics: A new frontier in Earth science research: Reviews of Geophysics, **47**, RG4004, doi: 10.1029/2009RG000285.

Bohuon, P., M. Le Maguer, and A. L. Raoult-Wack, 1997, Densities and viscosities of ternary systems of NaCl–sucrose–water from 283.15 to 303.15 K: Journal of Chemical and Engineering Data, **42**, 266–269, doi: 10.1021/je960226a.

Davis, C. A., L. J. Pyrak-Nolte, E. A. Atekwana, D. D. Werkema, and M. E. Haugen, 2009, Microbial-induced heterogeneity in the acoustic properties of porous media: Geophysical Research Letters, **36**, L21405, doi: 10.1029/2009GL039569.

Davis, C. A., L. J. Pyrak-Nolte, E. A. Atekwana, D. D. Werkema, and M. E. Haugen, 2010, Acoustic and electrical property changes due to microbial growth and biofilm formation in porous media: Journal of Geophysical Research, **115**, G00G06, doi: 10.1029/2009JG001143.

DeJong, J. T., M. B. Frtzges, and K. Nusslein, 2006, Microbially induced cementation to control sand response to undrained shear: Journal of Geotechnical and Geoenvironmental Engineering, **132**, 1381–1392, doi: 10.1061/(ASCE)1090-0241(2006)132:11(1381).

Dvorkin, J., R. Nolenhoeksema, and A. Nur, 1994, The squirt-flow mechanism — Macroscopic description: Geophysics, **59**, 428–438, doi: 10.1190/1.1443605.

Gray, M. R., A. Yeung, and J. M. Foght, 2008, Potential microbial enhanced oil recovery processes: A critical analysis: Presented at 2008 Society of Petroleum Engineers Annual Technical Conference and Exhibition.

Jack, T. R., 1991, Microbial enhancement of oil recovery: Current Opinion in Biotechnology, **2**, 444–449, doi: 10.1016/S0958-1669(05)80154-5.

Johnson, D. L., J. Koplik, and R. Dashen, 1987, Theory of dynamic permeability and tortuosity in fluid-saturated porous media: Journal of Fluid Mechanics, **176**, 379–402, doi: 10.1017/S0022112087000727.

Kato, S., T. Suzuki, H. Nomura, and Y. Miyahara, 1980, Ultrasonic relaxation in aqueous solutions of dextran: Macromolecules, **13**, 889–892, doi: 10.1021/ma60076a024.

Lappan, R. E., and H. S. Fogler, 1994, *Leuconostoc mesenteroides* growth kinetics with application to bacterial profile modification: Biotechnology and Bioengineering, **43**, 865–873, doi: 10.1002/bit.260430905.

Lappan, R. E., and H. S. Fogler, 1996, Reduction of porous media permeability from in situ *Leuconostoc mesenteroides* growth and dextran production: Biotechnology and Bioengineering, **50**, 6–15, doi: 10.1002/(SICI)1097-0290(19960405)50:1<6::AID-BIT2>3.0.CO;2-L.

Mavko, G. M., and A. Nur, 1979, Wave attenuation in partially saturated rocks: Geophysics, **44**, 161–178, doi: 10.1190/1.1440958.

Naessens, M., A. Cerdobbel, W. Soetaert, and E. J. Vandamme, 2005, *Leuconostoc* dextransucrase and dextran: Production, properties, and applications: Journal of Chemical Technology and Biotechnology, **80**, 845–860, doi: 10.1002/jctb.1322.

Padmanabhan, P. A., D. S. Kim, D. Pak, and S. J. Sim, 2003, Rheology and gelation of water-insoluble dextran from *Leuconostoc mesenteroides* NRRL B-523: Carbohydrate Polymers, **53**, 459–468, doi: 10.1016/S0144-8617(03)00140-1.

Prasad, M., and R. Meissner, 1992, Attenuation mechanisms in sands: Laboratory versus theoretical (Biot) data: Geophysics, **57**, 710–719, doi: 10.1190/1.1443284.

Quan, Y. L., and J. M. Harris, 1997, Seismic attenuation tomography using the frequency shift method: Geophysics, **62**, 895–905, doi: 10.1190/1.1444197.

Radlinski, A. P., E. Z. Radlinska, M. Agamalian, G. D. Wignall, P. Lindner, and O. G. Randl, 1999, Fractal geometry of rocks: Physical Review Letters, **82**, 3078–3081, doi: 10.1103/PhysRevLett.82.3078.

Rebata-Landa, V., and J. C. Santamarina, 2012, Mechanical effects of biogenic nitrogen gas bubbles in soils: Journal of Geotechnical and Geoenvironmental Engineering, **138**, 128–137, doi: 10.1061/(ASCE)GT.1943-5606.0000571.

Sears, F. M., and B. P. Bonner, 1981, Ultrasonic attenuation measurement by spectral ratios utilizing signal processing techniques: IEEE Transactions on Geoscience and Remote Sensing, **GE-19**, 95–99, doi: 10.1109/TGRS.1981.350359.

Shukla, R., S. Shukla, V. Bivolarski, I. Iliev, I. Ivanonva, and A. Goyal, 2011, Structural characterization of insoluble dextran produced by *Leuconostoc mesenteroides* NRRL B-1149 in the presence of maltose: Food Technology and Biotechnology, **49**, 291–296.

Stenekes, R. J. H., H. Talsma, and W. E. Hennink, 2001, Formation of dextran hydrogels by crystallization: Biomaterials, **22**, 1891–1898, doi: 10.1016/S0142-9612(00)00375-6.

Stewart, T. L., and H. S. Fogler, 2001, Biomass plug development and propagation in porous media: Biotechnology and Bioengineering, **72**, 353–363, doi: 10.1002/1097-0290(20010205)72:3<353::AID-BIT13>3.0.CO;2-U.

Taylor, S. W., and P. R. Jaffé, 1990, Biofilm growth and the related changes in the physical-properties of a porous-medium .1. Experimental investigation: Water Resources Research, **26**, 2153–2159, doi: 10.1029/WR026i009p02153.

Toksöz, M. N., D. H. Johnston, and A. Timur, 1979, Attenuation of seismic waves in dry and saturated rocks: I. Laboratory measurements: Geophysics, **44**, 681–690, doi: 10.1190/1.1440969.

van Dalen, K.N., R. Ghose, G. G. Drijkoningen, and D. M. J. Smeulders, 2010, In-situ permeability from integrated poroelastic reflection coefficients: Geophysical Research Letters, **37**, L12303, doi: 10.1029/2010GL043319.

van Paassen, L., R. Ghose, T. van der Linden, W. van der Star, and M. van Loosdrecht, 2010, Quantifying biomediated ground improvement by ureolysis: Large-scale biogrout experiment: Journal of Geotechnical and Geoenvironmental Engineering, **136**, 1721–1728, doi: 10.1061/(ASCE)GT.1943-5606.0000382.

Williams, K. H., D. Ntarlagiannis, L. D. Slater, A. Dohnalkova, S. S. Hubbard, and J. F. Banfield, 2005, Geophysical imaging of stimulated microbial biomineralization: Environmental Science and Technology, **39**, 7592–7600, doi: 10.1021/es0504035.

Youssef, N., M. S. Elshahed, and M. J. McInerney, 2009, Microbial processes in oil fields: Culprits, problems and opportunities: Advances in Applied Microbiology, **66**, 141–251, doi: 10.1016/S0065-2164(08)00806-X.